NJC

ROYAL SOCIETY OF CHEMISTRY

PAPER

View Article Online
View Journal | View Issue

Cite this: *New J. Chem.*, 2022, **46**, 10012

When ring makes the difference: coordination properties of Cu^{2+}/Cu^{+} complexes with sulfur-pendant polyazamacrocycles for radiopharmaceutical applications†

Marianna Tosato,[a] Matteo Pelosato,[a] Sara Franchi,[a] Abdirisak Ahmed Isse,[a] Nóra Veronica May,[b] Giordano Zanoni,[a] Fabrizio Mancin,[a] Paolo Pastore,[a] Denis Badocco,[a] Mattia Asti[c] and Valerio Di Marco *[a]

Three polyazamacrocyclic ligands, *i.e.* 1,5,9-tris[2-(methylsulfanyl)ethyl]-1,5,9-triazacyclododecane (TACD3S), 1,4,7,10-tetrakis[2-(methylsulfanyl)ethyl]-1,4,7,10-tetrazacyclotridecane (TRI4S) and 1,4,8,11-tetrakis[2-(methylsulfanyl)ethyl]-1,4,8,11-tetrazacyclotetradecane (TE4S), were considered as potential chelators for the medically relevant copper radioisotopes. The ligands have been synthesized through facile, single-step reactions, and their acidity constants have been measured in aqueous solution at 25 °C. The kinetic, thermodynamic, electrochemical and structural properties of their Cu^{2+} and Cu^{+} complexes were investigated in aqueous solution at 25 °C using spectroscopic (UV-Visible, EPR, NMR) and electrochemical techniques (pH-potentiometric titrations, cyclic voltammetry and electrolysis). TACD3S was demonstrated to be unable to stabilize Cu^{2+}, whereas for TRI4S and TE4S the formation of stable monocupric (CuL^{2+}) and monocuprous (CuL^{+}) complexes was detected. TRI4S coordinates Cu^{2+} *via* a [4N] and a [4N]S array of donor atoms while with TE4S only the latter geometry exists. The thermodynamic stability and the kinetic inertness of the copper complexes formed by TACD3S, TRI4S and TE4S were compared with those previously reported for 1,4,7,10-tetrakis-[2-(methylsulfanyl)ethyl]-1,4,7,10-tetrazacyclododecane (DO4S) to unravel the influence of the ring size and the nitrogen donor array on the copper chelation properties of these sulfur-rich macrocycles. The copresence of four nitrogen atoms is an essential feature to allow effective copper coordination when a 12-member ring is employed, as the Cu^{2+}–DO4S complexes were far more stable than those of Cu^{2+}–TACD3S. Furthermore, the larger ring size of TRI4S and TE4S, when compared to DO4S, progressively increases the rate of the Cu^{2+} complexation reactions but decreases the thermodynamic stability of the Cu^{2+} complexes. Despite this, the ability of TRI4S and TE4S to stably accommodate both copper oxidation states makes them very attractive for application in nuclear medicine as they could avoid the demetallation after the biologically triggered Cu^{2+}/Cu^{+} reduction.

Received 1st March 2022,
Accepted 22nd April 2022

DOI: 10.1039/d2nj01032a

rsc.li/njc

Introduction

A great deal of progress toward patient-specific treatment has been made in recent years sparked by the theranostic approach, in which a radioactive drug is used to diagnose and subsequently treat cancer.[1] Among the medically useful candidate radiometals, copper perfectly matches this philosophy as it possesses a unique combination of isotopes capable of both imaging and therapy. Copper-64 (^{64}Cu, $t_{1/2}$ 12.7 h) decays through a combination of electron capture (I_{EC} 43%), β^- ($I_{\beta-}$ 39%, $E_{\beta-,max}$ 573 keV) and β^+ ($I_{\beta+}$ 18%, $E_{\beta+,max}$ 655 keV) emission, which makes it suitable for both positron emission tomography (PET) imaging and radiotherapy.[2–5] On the other hand, copper-67 (^{67}Cu, $t_{1/2}$ 61.9 h) is a promising candidate for therapy as well as for single photon emission computed tomography (SPECT) imaging due to its β^- ($I_{\beta-}$ 100%, $E_{\beta-,max}$ 141 keV) and γ-rays emission (E_γ 93 keV, I_γ 16%; E_γ 185 keV, I_γ 49%).[6–8]

The stable complexation through a bifunctional chelator (BFC) covalently tethered to a targeting biomolecule is imperative to securely deliver $[^{64/67}Cu]Cu^{2+}$ to tumour cells.[9–11] The Cu^{2+}-BFC

[a] *Department of Chemical Sciences, University of Padova, 35131 Padova, Italy. E-mail: valerio.dimarco@unipd.it*
[b] *Centre for Structural Science, Research Centre for Natural Sciences, 1117 Budapest, Hungary*
[c] *Radiopharmaceutical Chemistry Section, Nuclear Medicine Unit, AUSL-IRCCS di Reggio Emilia, 42122 Reggio Emilia, Italy*

† Electronic supplementary information (ESI) available. See DOI: https://doi.org/10.1039/d2nj01032a

complex must possess high thermodynamic stability and kinetic inertness to avoid the release of the radiometal *in vivo*. Particularly, the biologically-induced reduction of Cu^{2+} to Cu^{+} is a potential pathway for the demetallation of $[^{64/67}Cu]Cu^{2+}$ radioconjugates, as unstable and labile cuprous species can trigger the dissociation of the complexes.[2,12–15] As a result, the unbound radiometal can spread through the body leading to a loss of selectivity for the target to be imaged or treated.[15]

Despite the huge number of BFCs that have been evaluated for $[^{64/67}Cu]Cu^{2+}$ complexation, chelating ligands able to simultaneously coordinate both 2+ and 1+ copper oxidation states have received markedly less attention.[16–18] Given the borderline character of Cu^{2+} according to Pearson's Hard–Soft Acid–Base theory (HSAB), the investigated BFCs for its chelation are mostly confined to polyazamacrocyclic scaffolds with pendant carboxylate arms such as 1,4,7,10-tetraazacyclododecane-1,4,7,10-tetraacetic acid (DOTA), 1,4,8,11-tetraazacyclotetradecane-1,4,8,11-tetraacetic acid (TETA) and their derivatives (Fig. 1). These ligands form thermodynamically stable complexes with Cu^{2+} but suffer from *in vivo* demetalation.[13,19–21] Variation of the ring structure and/or the substituents afforded more stable and inert cross-bridged systems like 1,4,8,11-tetraazabicyclo[6.6.2]-hexadecane-4,11-diacetic acid (CB-TE2A) and 1,4,7,10-tetraazabicyclo[5.5.2] tetradecane-4,10-diacetic acid (CB-DO2A) (Fig. 1), but their sluggish radiolabeling kinetics necessitated the use of harsh protocols, hampering their use for thermally-sensitive molecule labelling.[21–24] Generally promising results have been obtained with 1,4,7-triazacyclononane-1,4,7-triacetic acid (NOTA) and its 1-glutaric acid derivative (NODAGA).[5] However, the development of $[^{64/67}Cu]Cu^{2+}$ chelators combining high *in vivo* stability and kinetic inertness toward transmetallation, transchelation and reduction to Cu^{+} remains a challenge.[13,25,26]

We have recently reported the evaluation of a series of sulfur-containing cyclen derivatives as chelators for $[^{64/67}Cu]Cu^{2+/+}$ which exhibited very high thermodynamic stability for both copper oxidation states.[27] The design of this ligand series was based on the idea that the presence of S, N, and O donors would allow the coordination of both Cu^{2+} and Cu^{+}. This "first generation" series consisted of 1,4,7,10-tetrakis[2-(methylsulfanyl)ethyl]-1,4,7,10-tetraazacyclododecane (DO4S), 1,4,7-tris[2-(methylsulfanyl)ethyl]-1,4,7,10-tetraazacyclododecane (DO3S), 1,4,7-tris[2-(methylsulfanyl)ethyl]-10-acetamido-1,4,7,10-tetraazacyclododecane (DO3SAm) and 1,7-bis[2-(methylsulfanyl)ethyl]-4,10,diacetic acid-1,4,7,10-tetraazacyclododecane (DO2A2S) (Fig. 1).[27,28]

Based on this promising strategy, we decided to expand the family of sulfur-based polyazamacrocyclic ligands to evaluate the impact of a larger macrocyclic ring and a different number of N/S donor atoms on the thermodynamic, kinetic, and redox properties of their cupric and cuprous complexes. For this purpose, we have considered a "second generation" series of polyazamacrocycles incorporating sulfanyl pendant arms. 1,5,9-Tris[2-(methylsulfanyl)ethyl]-1,5,9-triazacyclododecane (TACD3S) possesses the same number of atoms in the ring as DO4S but fewer overall donors (3N3S *vs.* 4N4S), while 1,4,7,10-tetrakis[2-(methylsulfanyl)ethyl]-1,4,7,10-tetrazacyclotridecane (TRI4S) and 1,4,8,11-tetrakis[2-(methylsulfanyl)ethyl]-1,4,8,11-tetrazacyclotetradecane (TE4S) have the same number of nitrogen and sulfanyl pendants as DO4S but a progressively larger ring size (Fig. 1). To the best of our knowledge, TACD3S and TRI4S are novel

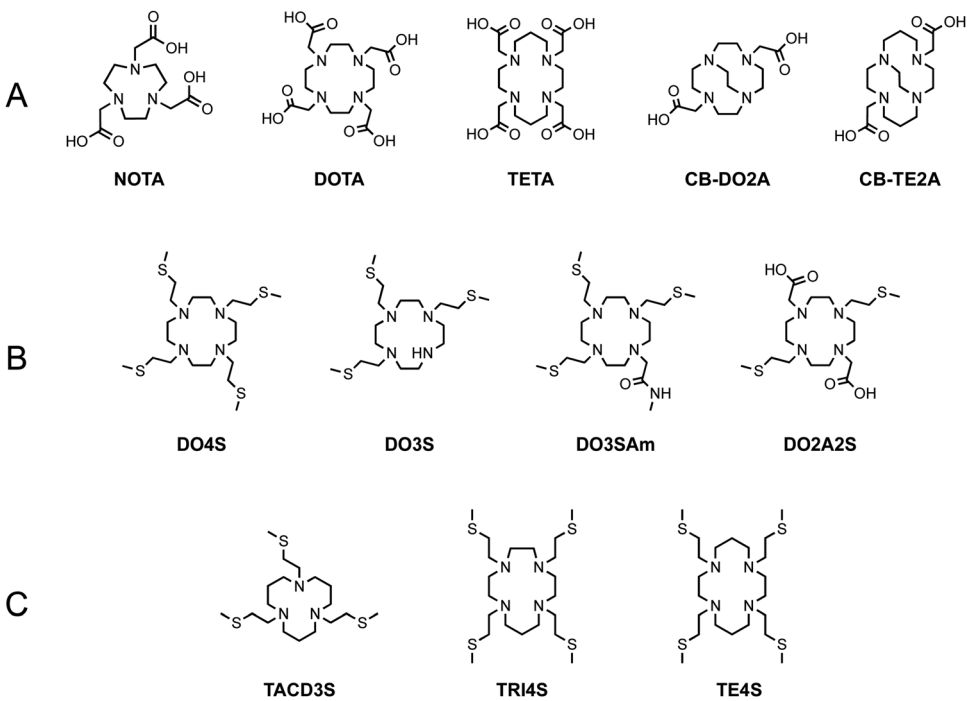

Fig. 1 (A) Representative state-of-the-art ligands for copper radioisotopes chelation. The (B) "first" and (C) "second generation" series of sulfur-bearing ligands developed by our group.[27]

ligands, whereas TE4S has been considered by Schmid *et al.*,[29] who however only investigated the solid-state structure and not the aqueous solution chemistry of its Cu^{2+} complexes. It is worth mentioning that the complex formation of Cu^{2+} or of other metal ions was investigated very rarely with polyazamacrocycles bearing sulfur-containing pendant arms, and when this was done, the investigated molecules contained only one sulfur side chain, or were based on different rings than cyclen, 1,4,7,10-tetrazacyclotridecane (TRI), and cyclam.[30–33]

The investigation of the acid–base and Cu^{2+}/Cu^{+} complexation properties of TACD3S, TRI4S and TE4S in aqueous solution was performed herein using a combination of spectroscopic (UV-Vis, EPR and NMR) and electrochemical techniques (potentiometry, cyclic voltammetry and electrolysis). The final aim of investigating this series of sulfur-pendant polyazamacrocycles is to unravel the physicochemical properties of their copper complexes, in order to rationalize the alterations induced by the reported structural modifications, and thus guide the design of improved copper chelators for radiopharmaceutical applications.

Experimental

Materials

All reagents and solvents were obtained from commercial suppliers (Sigma Aldrich, VWR Chemicals) and were used as received. 1,5,9-Triazacyclododecane (TACD), 1,4,7,10-tetrazacyclotridecane (TRI), 1,4,7,10-tetrazacyclododecane (cyclen) and 1,4,8,11-tetrazacyclotetradecane (cyclam) were purchased from Chematech. All solutions were prepared with ultrapure water (18.2 MΩ cm^{-1}) which was purified with a Purelab Chorus (Veolia) system.

Ligand synthesis

All ligands were synthesized starting from the unsubstituted macrocyclic ring, potassium carbonate and acetonitrile (15 mL) mixed in a pressure tube flushed with nitrogen.

2-Chloroethyl methyl sulfide was added and the pressure tube was heated to 60 °C under stirring for 24 h. The mixture was then evaporated under reduced pressure. All products were purified by flash column chromatography on silica (60 Å, 230–400 mesh, 40–63 μm, Sigma-Aldrich) using $CHCl_3$: CH_3OH 9 : 1 + 0.5% $NH_{3(aq)}$ 30% as the eluent and collected as a yellowish paste. NMR spectra were recorded using a Bruker AV III 500 spectrometer operating at 500 MHz for ^1H and 125.8 MHz for $^{13}C\{^1H\}$. Chemical shifts (δ) were reported as parts per million (ppm) relative to the residual solvent peak and coupling constants (J) in hertz (Hz). Multiplicity is given as follows: s = singlet, d = doublet, t = triplet, q = quartet, qn = quintet, m = multiplet, and br = broad peak. High-resolution mass spectra (HRMS, ESI) were recorded with an Agilent Technologies LC/MSD Trap SL mass spectrometer.

In the following, the reactant and product amounts are given for each compound together with the spectral data.

1,5,9-Tris[2-(methylsulfanyl)ethyl]-1,5,9-triazacyclododecane (TACD3S). 1,5,9-Triazacyclododecane (171 mg, 1.0 mmol, 1.0 eq.), potassium carbonate (989 mg, 6.5 mmol, 6.5 eq.), 2-chloroethyl methyl sulfide (399 μL, 4.0 mmol, 4.0 eq.). TACD3S: 247 mg, 0.63 mmol, 63% yield. ^1H NMR (500 MHz, $CDCl_3$): δ 2.59 (s, CH_2CH_2S, 12H), 2.53 (t, NCH_2, J = 6.13 Hz, 12H), 2,11 (s, SCH_3, 9H), 1.59 (qn, CH_2, J = 12.3 Hz, 6H). $^{13}C\{^1H\}$ NMR (126 MHz, $CDCl_3$): δ 53.36 (NCH_2CH_2S), 49.23 ($NCH_2CH_2CH_2N$), 32.14 (NCH_2CH_2S), 21.40 ($NCH_2CH_2CH_2N$), 15.81 (SCH_3). HRMS (ESI) m/z [M + H^+]: 394.2478; calc: 394.2379.

1,4,7,10-Tetrakis[2-(methylsulfanyl)ethyl]-1,4,7,10-tetrazacyclotridecane (TRI4S). 1,4,7,10-Tetraazacyclotridecane (448 μL, 1.0 mmol, 1.0 eq.), potassium carbonate (898 mg, 6.5 mmol, 6.5 eq.), 2-chloroethyl methyl sulfide (448 μL, 4.5 mmol, 4.5 eq.). TRI4S: 182 mg, 3.8 mmol, 38% yield. ^1H NMR (500 MHz, $CDCl_3$): δ 2.73–2.58 (m, 32H, CH_2), 2.169 (s, 6H, SCH_3), 2.167 (s, 6H, SCH_3), 1.63 (t, J = 12.30 Hz, 2H, $NCH_2\underline{CH_2}CH_2N$). $^{13}C\{^1H\}$ NMR (126 MHz, $CDCl_3$): δ 54.98 (CH_2), 54.58 (CH_2), 52.46 (CH_2), 52.35 (CH_2), 51.63 (CH_2), 50.95 (CH_2), 31.89 (CH_2SCH_3), 31.65 (CH_2SCH_3), 23.35 ($NCH_2\underline{CH_2}CH_2N$), 15.86 ($SCH_3$). HRMS (ESI) m/z [M + H^+]: 483.2784; calc. 483.2678.

1,4,8,11-Tetrakis[2-(methylsulfanyl)ethyl]-1,4,8,11-tetrazacyclotetradecane (TE4S). 1,4,8,11-Tetraazacyclotetradecane (200 mg, 1 mmol, 1 eq.), potassium carbonate (1.17 g, 8.5 mmol, 8.5 eq.), 2-chloroethyl methyl sulfide (528 μL, 5.3 mmol, 5.3 eq.). TE4S: 211 mg, 0.42 mmol, 42% yield. ^1H NMR (500 MHz, $CDCl_3$): δ 2.81–2.69 (m, 32H, CH_2), 2.22 (s, 12H, SCH_3), 1.77 (qn, J = 13.80 Hz, 4H, $NCH_2\underline{CH_2}CH_2N$). $^{13}C\{^1H\}$ NMR (126 MHz, $CDCl_3$): δ 54.56 (CH_2), 51.22 (CH_2), 50.39 (CH_2), 31.23 (CH_2SCH_3), 23.01 ($NCH_2\underline{CH_2}CH_2N$), 14.46 ($SCH_3$). HRMS (ESI) m/z [M + H^+]: 497.2935; calc. 497.2835.

DO4S and DO2A2S. 1,4,7,10-Tetrakis[2-(methylsulfanyl)ethyl]-1,4,7,10-tetraazacyclododecane (DO4S) and 1,7-bis[2-(methylsulfanyl)ethyl]-4,10,diacetic acid-1,4,7,10-tetraazacyclododecane (DO2A2S) were synthesized in our laboratories according to previously reported procedures.[28]

Formation kinetics

The formation kinetics of Cu^{2+} complexes with the investigated ligands was monitored as a function of pH at room temperature *via* UV-Vis spectroscopy, following the increasing intensity of the charge transfer and/or d–d bands of the complexes at the characteristic wavelengths. The electronic spectra were recorded in the 200–800 nm range at different time points using a Cary 60 UV-Visible spectrophotometer (Agilent) equipped with a 1 cm path length quartz cell. Complexation kinetics experiments were carried out by mixing equimolar amounts of metal and ligand solutions (final concentrations: $C_{Cu^{2+}} = C_L = 10^{-4}$ M) in a buffered medium at pH 2 (HCl 10^{-2} M), pH 3.7 (acetic/acetate buffer) and pH 7.5 (2-[4-(2-hydroxyethyl)piperazin-1-yl]ethane sulfonic acid – HEPES – buffer).

Protonation and metal–ligand stability constants

Potentiometric titrations. The potentiometric measurements were performed as previously described.[27,28,34] Briefly, an automated titrating system (Metrohm 765 Dosimat) with a combined glass electrode (Hamilton pH 0–14) and a Metrohm 713 pH-meter were used. The measurements were carried out in a

thermostated jacketed cell at 25.0 ± 0.2 °C and kept under a nitrogen atmosphere during the titrations to remove CO_2. A constant ionic strength of 0.15 M $NaNO_3$ was used.

0.1 M nitric acid stock solutions (Aristar – VWR Chemicals) were prepared from a concentrated one and standardised against sodium carbonate (Aldrich, 99.95–100.5%). 0.1 M sodium hydroxide solutions with a low carbonate content were prepared from commercial pellets (Fluka, 99% min) and their accurate concentrations were obtained by titration of the previously standardized HNO_3 solutions. Stock solutions of the ligands and Cu^{2+} were freshly prepared by direct dissolution of the synthesized compounds ($\sim 10^{-3}$ M) and from analytical-grade $Cu(NO_3)_2{\cdot}3H_2O$ (Sigma Aldrich) ($\sim 10^{-2}$ M), respectively. HNO_3 ($C_{H^+} = 4.2{\cdot}C_L$) was coadded to the ligand solution to avoid carbonatation and facilitate dissolution. The solubility of the ligands in water depends on pH, and in all cases minimal values occur at pH > 9 where the non-charged, totally deprotonated form L predominates. The limit solubility of L was estimated from the pH at which precipitation starts, knowing the pK_a values of each ligand (see below) and the stoichiometric ligand concentration: the results for TACD3S, TRI4S and TE4S were 1.5×10^{-4} M, 1.9×10^{-4} M and 1.3×10^{-4} M, respectively.

The concentration of the ligands in the titration vessel ranged from 7×10^{-4} M to 2×10^{-3} M while the metal:ligand ratio varied from 1:1 to 1:2. The ligand solutions were acidified with a known volume of HNO_3, followed by the addition of Cu^{2+} in the case of the metal–ligand titrations, and the titrations were then carried out by adding known volumes of NaOH. The purity of the synthesized chelators was demonstrated to be adequate (> 95%). The explored pH range was 2–12 except for Cu^{2+}–TRI4S where the titrations were started at pH ∼ 4 to avoid too slow complexation kinetics. Each titration was performed independently at least in triplicate.

NMR titrations. NMR spectra of the free ligands at different pH were collected at 25 °C using a 400 MHz Bruker Avance III HD spectrometer. Chemical shifts (δ) are reported in parts per million (ppm) and are referred to 3-(trimethylsilyl) propionic acid sodium salt (Sigma Aldrich, 99%). The solutions were prepared in H_2O + 10% D_2O (Sigma Aldrich, 99.9% D) at a concentration of $\sim 10^{-3}$ M. The pH was adjusted with small additions (μL) of HNO_3 and/or NaOH and measured with the same pH-meter and electrode as those used for the potentiometric measurements. The water signal was suppressed using an excitation sculpting pulse scheme.[35] All data were collected and processed with Topspin 3.5 using standard Bruker processing parameters with Topspin 4.1.1 software.

UV-Vis titrations. Out-of-cell and in-cell UV-Vis spectrophotometric titrations were performed to determine the stability constants of the Cu^{2+} complexes. In the first method, separate samples in the pH range 0–4 were prepared by mixing equimolar amounts of ligand and Cu^{2+} at final concentrations $C_{Cu^{2+}} = C_L = 10^{-4}$ M (the copper stock solutions were prepared from $CuCl_2{\cdot}2H_2O$, Sigma-Aldrich, 99.9%), and a known amount of previously standardized HCl (Sigma-Aldrich, 37%) to adjust the pH. The pH was measured using a combined glass electrode (Mettler Toledo pH-meter) daily calibrated with commercial buffer solutions (pH 4.01 and 7.01 at 25 °C). In highly acidic solutions (pH < 2), the pH was computed from the HCl concentration ($pH = -\log C_{HCl}$). The absorption spectra were collected in the spectral range 200–800 nm using a 1 cm path length quartz cuvette and using the same spectrometer of the kinetic measurements. The equilibrium was reached when no variations of both the electronic spectra and the pH were detected.

Between pH 4 and 12, direct titrations were carried out. Typically, equimolar metal-to-ligand solutions were mixed (final concentrations: $C_{Cu^{2+}} = C_L = 10^{-4}$ M), the pH was adjusted to ∼ 4, and the titrations were carried out by adding a known volume of NaOH, similarly to the pH-potentiometric titrations. After each addition, the pH was allowed to equilibrate, an aliquot was transferred to the spectrophotometric cell and the spectrum was recorded. Then, the aliquot was transferred back to the titration vessel and a new addition was made. The maximum pH value was ∼ 12. Typical titrand and titrant volumes were in the range 10–25 mL and less than 100 μL, respectively. The same protocol was used for the determination of the ligand protonation constants but, in this case, no Cu^{2+} was added.

Stoichiometry of Cu^{2+} complexes. The stoichiometry of the Cu^{2+} complexes was determined by adding different aliquots of Cu^{2+} solution to the chelator one ($C_L = 10^{-4}$ M) buffered at pH 7.5 by HEPES to obtain a metal-to-ligand ratio varying from 0:1 to 3:1. After Cu^{2+} additions, the UV-Vis spectra were recorded, and the stoichiometry was determined by plotting the absorbance at the characteristic wavelengths as a function of the metal-to-ligand ratios.

Data treatment. The protonation constants and the stability constants were refined using the least-squares fitting program PITMAP.[36] The programme minimises the sum of the squares of the differences between experimental and calculated values. Optimization is performed using pitmapping or simplex as nonlinear least squares algorithms.[37,38] Mass balance equations are solved, *i.e.* species concentration at equilibrium are obtained, by means of the Newton–Raphson method.[38] All equilibrium constants were defined as cumulative formation constants ($\log \beta_{pqr} = [M_pL_qH_r]/[M]^p[L]^q[H]^r$) and are therefore referred to the overall equilibrium $pM^{m+} + qH^+ + rL^{l-} \leftrightarrows M_pH_qL_r^{pm+q-rl}$, where the metal and ligand are designated as M and L, respectively.[36] The refinements of the overall formation constants included, in each case, the previously determined ligand protonation constants and the metal hydrolysis products, whose equilibrium constants were fixed to the literature values.[39] The errors quoted are the standard deviations calculated by the PITMAP program.[36] The following parameters, which strongly correlated with each other, were calculated by the same program from acid–base titrations, and then kept constant in subsequent ligand and Cu^{2+}–ligand titrations: water ionization constant (pK_w), glass electrode alkaline error (given by the selectivity coefficient for Na^+, pk_{Na}), and carbonatation degree of the NaOH solution (%), which were 13.54, 12.0 and 0.5% on average, respectively.

EPR

X-band CW-EPR spectra were recorded with a Bruker EleXsys E500 spectrometer (microwave frequency 9.4 GHz, microwave

power 13 mW, modulation amplitude 5 G, modulation frequency 100 kHz).

The Cu^{2+}–TE4S sample was prepared the day before the measurement and stirred overnight at room temperature to take into account the slow kinetics of complex formation. pH-Dependent EPR spectra were measured in the pH range 1.86–11.47. NaOH or HCl were employed to adjust the pH.

Room temperature EPR spectra were recorded in capillaries using six scans. Room temperature spectra were corrected with the background spectrum of pure aqueous solution before the simulation. Frozen solution EPR spectra were measured in quartz EPR tubes placed into Dewar containing liquid nitrogen at 77 K. 0.2 mL of sample was placed in the tube and 0.05 mL methanol was added to avoid the crystallization of water. All CW-EPR spectra were simulated by the EPR software.[40] Room temperature spectra were described by the isotropic EPR parameters g_o and A_o^{Cu} copper hyperfine couplings, and the relaxation parameters α, β, and γ which define the linewidths in the equation $\sigma_{MI} = \alpha + \beta M_I + \gamma M_I^2$, where M_I denotes the magnetic quantum number of the copper nucleus. The super hyperfine coupling (a_0^N) of four equivalent nitrogen atoms significantly improved the fit. The anisotropic spectra were analysed with the help of axial *g*- and *A*-tensor values ($g_\perp$, $g_\parallel$, $A_\perp^{Cu}$, $A_\parallel^{Cu}$) and the orientation-dependent linewidth parameters. Since natural $CuCl_2$ was used for the measurements, the spectra were calculated as the sum of the spectra of ^{63}Cu and ^{65}Cu weighted by their natural abundances. The copper and nitrogen coupling constants and the relaxation parameters were obtained in field units (Gauss = 10^{-4} T).

Stability/inertness with competitive metal cations

Different aliquots of Zn^{2+} and Ni^{2+} solutions were added to a solution of the preformed cupric complexes ($C_{CuL^{2+}} = 10^{-4}$ M) to obtain the following $n(M^{2+})/n(CuL^{2+})$ ratios: $50 \leq n(Zn^{2+})/n(CuL^{2+}) \leq 1000$ and $50 \leq n(Ni^{2+})/n(CuL^{2+}) \leq 250$. The spectral variations induced by the addition of the competitor were monitored at room temperature using UV-Vis spectroscopy for 5 days.

Acid-mediated decomplexation kinetics

Acid-mediated decomplexation studies of the Cu^{2+} complexes were performed under pseudo-first-order conditions in 0.1–1 M HCl at 25 °C ($C_{CuL^{2+}} = 10^{-4}$ M). The reactions were monitored by UV-Vis spectroscopy following the decrease in intensity of the charge transfer transitions of the Cu^{2+} complexes at the characteristic wavelength at specific time points. The $^{d}k_{obs}$ values were calculated from the experimental data by using a single-exponential model $A(t) = A(0)\cdot e^{-^{d}k_{obs}\cdot t}$. The corresponding half-life was obtained from the equation $t_{1/2} = \ln(2)/^{d}k_{obs}$.

Cyclic voltammetry

Cyclic voltammetry was carried out in aqueous solution at room temperature with an Autolab PGSTAT 302N potentiostat operated with NOVA 2.1 (Metrohm) data acquisition software. The experiments were performed with a six-neck glass cell using a glassy carbon (GC) working electrode (WE) fabricated from a 3 mm-diameter rod (Tokai GC-20), a saturated calomel reference electrode (SCE) and a platinum wire counter electrode (CE). The WE surface was routinely polished with 0.25 μm diamond paste, followed by ultrasonic rinsing in ethanol for 5 minutes before use.

The sample solutions containing the copper complexes were degassed by bubbling Ar before all measurements and kept under an Ar blanket throughout the measurements. 0.15 M $NaNO_3$ was used as a supporting electrolyte and the pH was adjusted with NaOH and HNO_3 solutions.

Cyclic voltammograms with scan rates ranging from 0.01 to 0.1 V s^{-1} were recorded in the region from −0.5 to 0.5 V. In this potential range, the solvent, the background electrolyte, and the ligands were electrochemically inactive.

Electrolysis and NMR

Exhaustive electrolyses of the pre-formed Cu^{2+} complexes were carried out using large area glassy carbon WE in a two-compartment cell. The CE was a Pt gauze in 0.15 M $NaNO_3$ solution, separated from the WE solution by two glass frits (G3). A saturated calomel electrode was used as a reference electrode. The electrolyses were performed at a fixed potential equal to $E = -0.45$ V and $E = -0.40$ V for Cu^{2+}–TRI4S and Cu^{2+}–TE4S, respectively. Linear scan voltammetry (LSV) on a rotating disc electrode was used to monitor the evolution of the species in solution. Each electrolysis was considered complete when the cathodic current reached $\lesssim$2% of the initial value.

^{1}H-NMR spectra of the *in situ* generated Cu^+ complexes were collected at 25 °C using the same spectrometer and the same protocol described above.

Results and discussion

Ligand synthesis

TACD3S, TRI4S and TE4S were synthesized by direct complete alkylation of the parent macrocycles with an excess of 2-chloroethyl methyl sulfide in acetonitrile at 60 °C for 24 hours according to Scheme S1 (ESI†).

Ligand protonation constants

Combined potentiometric, ^{1}H-NMR and UV-Vis spectrophotometric titrations in aqueous solution were used to determine the protonation constants of TACD3S, TRI4S and TE4S at 25.0 °C with the ionic strength adjusted to 0.15 M $NaNO_3$. The stepwise protonation constants (pK_a) are outlined in Table 1 and compared with those of DO4S and structurally related ligands (tetramethyl-cyclen and tetramethyl-cyclam) or with the parent unsubstituted macrocycles (1,5,9-triazacyclododecane – TACD, 1,4,7,10-tetrazacyclododecane – cyclen, 1,4,7,10-tetrazacyclotridecane – TRI and 1,4,8,11-tetrazacyclotetradecane – cyclam). The protonation speciation diagrams for TACD3S, TRI4S and TE4S are presented in Fig. S1 (ESI†).

For all the investigated chelators, the constants for the deprotonation of HL^+ and H_2L^{2+} (Table 1) can be assigned to the deprotonation of two opposite or adjacent nitrogen atoms

Table 1 Acidity constants (pK_a and $\log\beta$ values) of TACD3S, TRI4S and TE4S at T = 25 °C and I = 0.15 M $NaNO_3$. The pK_a values of the corresponding unsubstituted macrocycles and other structurally related compounds are reported for comparison purposes. Unless otherwise stated, the values were obtained by pH-potentiometry

Ligand	Equilibrium[a]			
	$HL^+ \rightleftharpoons L + H^+$	$H_2L^{2+} \rightleftharpoons HL^+ + H^+$	$H_3L^{3+} \rightleftharpoons H_2L^{2+} + H^+$	$L + 3H^+ \rightleftharpoons H_3L^{3+}$ [d]
TACD3S	9.60 ± 0.02; 9.6 ± 0.2[b]	5.57 ± 0.05; 5.41 ± 0.06[b]; 5.29 ± 0.03[c]	1.62 ± 0.07[b]	16.79
DO4S[ef]	10.14[e]	7.29[e]	1.9[f]	19.3
TRI4S	9.76 ± 0.03; 9.4 ± 0.1[b]	6.69 ± 0.03; 6.0 ± 0.3[b]; 6.10 ± 0.05[c]	1.5 ± 0.1[b]	18.0
TE4S	10.60 ± 0.01	7.73 ± 0.05; 7.5 ± 0.2[c]	1.7 ± 0.2[b]	20.0
TACD[g]	12.6	7.57	2.41	22.6
Cyclen[ef]	10.63[e]	9.51[e]	1.6[f]	21.7
Tetramethyl-cyclen[h]	11.06	8.95	—	20.01
TRI[i]	11.02	9.96	1.96	22.94
Cyclam[j]	11.3	10.23	1.43	23.0
Tetramethyl-cyclam[j]	9.34	8.99	2.58	20.91

[a] L represents the completely deprotonated form of each chelator. The reported uncertainty was obtained by the fitting procedure and represents one standard deviation unit. [b] Obtained from ^{1}H-NMR data, no ionic strength control. [c] Obtained from UV-Vis data, no ionic strength control. [d] The first pK_a value in each cell was considered for the $\log\beta$ computation. [e] From ref. 28, I = 0.15 M $NaNO_3$, T = 25 °C. [f] From ref. 27, no ionic strength control, T = 25 °C. [g] From ref. 41, I = 0.15 M KNO_3, T = 25 °C. [h] From ref. 42, I = 0.2 M $NaClO_4$, T = 25 °C. [i] From ref. 43, I = 0.1 M $NaNO_3$, T = 25 °C. [j] From ref. 44, I = 0.1 M $NaNO_3$, T = 25 °C.

of the azamacrocyclic rings. The other deprotonation constants (*i.e.* those for H_3L^{3+} and, if applicable, for H_4L^{4+}) were always found to be very high ($K_a > 10^{-2}$, *i.e.* $pK_a < 2$, Table 1), primarily due to the Coulombic repulsion between the positive charges resulting from the protonated amines that are forced into proximity by the cyclic nature of the ligands.

Comparing TRI4S and TE4S with DO4S, the slight differences in the pK_a values are related to the different ring sizes and the relative position of the nitrogen atoms. For TE4S, the higher pK_a values with respect to those of DO4S likely reflect the larger separation between the nitrogen atoms afforded by the larger backbone, which lowers the charge–charge repulsion, allowing better stabilization of the proton binding. On the contrary, the tertiary nitrogen atoms of TRI4S are less basic than those of DO4S and TE4S, indicating that the former molecule adopts conformers in which the ring protons are less stable than for the other two chelators. Simple charge–repulsion arguments do not explain this trend, which, as a tentative reason, might be ascribed to the asymmetry of TRI4S.

Although TACD3S and DO4S possess the same number of atoms in the macrocyclic scaffold, the former is significantly more acidic. In TACD3S the tertiary amines are separated by a larger distance with respect to DO4S, but the lower number of possible microstates (where protons are localized on different nitrogens) leads to lower stability of the protonated species for TACD3S, thus explaining the observed behaviour.

As previously found for DO4S and its derivatives,[28] a decrease of pK_a was also observed (especially for the deprotonation of H_2L^{2+})t with all the investigated sulfur-bearing ligands when compared to the bare macrocycles or the non-sulfanyl analogues. While the former effect can be explained by the consequence of the destabilization of the protonated species resulting from the decrease in water solvation after the *N*-alkylation, the latter was attributed to the presence of the sulfur atoms on the side arms.[28]

^{1}H-NMR spectroscopy was employed to confirm some pK_a values and to determine the most acidic ones ($pK_a \ll 2$) not accessible by potentiometric measurements. In addition, it was also used to gain insights into the solution structure and the dynamics of the protonation/deprotonation processes of the investigated ligands. The pK_a values determined by NMR are also reported in Table 1. Some minor discrepancies between the protonation constants obtained by NMR and potentiometry can be attributed to the uncontrolled ionic strength during NMR experiments.

The ^{1}H-NMR spectra of TACD3S, TRI4S and TE4S and the ^{1}H chemical shift variations as a function of pH are shown in Fig. S2–S4 and S5–S7 (ESI†). The signal assignments, supported by the bidimensional spectra of Fig. S8–S11 (ESI†), are reported in Tables S1–S3 (ESI†). A thorough description of the spectra is given in the ESI.

According to the sharpness of the signals and the absence of multiple patterns, all the deprotonation processes ($H_3L^{3+} \leftrightharpoons H_2L^{2+} + H^+ \leftrightharpoons HL^+ + H^+$) should be fast on the NMR timescale (Fig. S2–S4 and S12, ESI†). An exception is represented by the last deprotonation step of TACD3S, which appears markedly slower since both patterns of HL^+ and L, together with a signal enlargement, can be observed (Fig. S2, ESI†). The estimated molar ratio between these two species obtained by the integration of NMR signals is in good agreement with the values calculated by potentiometry. Moreover, the sharpness of the signals also indicates that the conformational equilibria within a single species are fast on the NMR timescale (except for TACD3S in its totally deprotonated form).

On the contrary, it is worth noting that in the cyclen-based analogue, *i.e.* DO4S, the multiplets were sharp only in its neutral form.[28] The lower energetic barrier of the conformer interconversion, resulting from the CH_2 spacer added in the ring of TACD3S, TRI4S and TE4S, could justify this difference.

As regards the UV-Vis analysis, the electronic spectra of TACD3S, TRI4S and TE4S display a strong absorption in the UV region (below 250 nm) which showed an absorbance increase close to the pK_a values (Fig. S13, ESI†), similarly to DO4S and its derivatives.[28] UV-Vis data were fitted to determine some pK_a values (Table 1) which agree reasonably well with those obtained from potentiometric titrations and NMR.

Cu^{2+} complexes: formation kinetics

The formation kinetics of the Cu^{2+} complexes with TACD3S, TRI4S and TE4S were assessed as a function of pH by UV-Vis spectroscopy, following the absorbance changes observed at selected wavelengths over time. This qualitative investigation was necessary to determine the timing required for reaching equilibrium, thus allowing the subsequent thermodynamic investigations.

For TRI4S and TE4S, reaction times from seconds to many hours were found (Fig. S14, S15 and Table S4, ESI†). The complex formation rate strongly decreased upon decreasing the pH, reflecting the dissimilar reactivity of the differently protonated ligand species predominating at different pH (Fig. S1, ESI†): higher protonation states correspond to the higher electrostatic repulsion between Cu^{2+} and the ring cavity where the donor atoms are located, as previously reported for DO4S and its derivatives.[27]

The increased ring size in TRI4S and TE4S significantly accelerates the formation of the Cu^{2+} complexes when compared with DO4S (Table S4, ESI†).[27] This complexation rate enhancement could be explained by the lower electrostatic repulsion between the metal ion and the nitrogen donors driven by the larger ring. TACD3S was found not to be able to complex Cu^{2+} except at nearly neutral pH (Fig. S15, ESI†), where the reaction rate was comparable to that of the other ligands.

Cu^{2+} complexes: thermodynamics

UV-Vis spectrophotometric titrations at equilibrium conditions were performed to determine the formation constants ($\log\beta$) of the Cu^{2+}-complexes with TACD3S, TRI4S and TE4S. The slow equilibration timing evidenced at acidic pH forced the use of out-of-cell titrations at pH $\leq$ 4 together with the direct in-cell ones (pH $>$ 4). The high binding Cu^{2+} affinity of TRI4S obviated the use of conventional pH-potentiometric techniques, while for TE4S pH-potentiometry was also employed.

As shown in Fig. S14 and S15 (ESI†), the Cu^{2+} addition to solutions containing any ligand causes the appearance of two absorption bands in the UV-Vis spectra, which are accountable for the metal complexation event. These bands change in intensity but not in shape with pH, so that the formation of the same Cu^{2+} complex in all the pH range was deduced. Fig. S16 (ESI†) shows the spectra at various pH; the fitting procedure indicated the presence of only one complex having stoichiometry CuL^{2+} (where L indicates the deprotonated ligand form). UV-Vis titrations at different metal-to-ligand molar ratios, which showed saturation at equimolar values (Fig. S17, ESI†), further confirmed this speciation model, whereas potentiometric titrations (at pH $\geq$ 2 for TE4S, at pH $\geq$ 4 for TRI4S) showed no protonation/deprotonation events occurring for the CuL^{2+} complexes in the investigated pH range. The overall stability constants are reported in Table 2 while the distribution diagrams are shown in Fig. 2 and Fig. S18 (ESI†).

The pCu^{2+} values ($pCu^{2+} = -\log[Cu^{2+}]_{free}$) were calculated at pH 7.4 to compare the chelating ability of the different ligands at physiological conditions: the higher the pCu^{2+}, the higher the stability of the complexes under the specified conditions.[45] The obtained values are listed in Table 2. As a comparison, the pCu^{2+} values for other DO4S derivatives and selected state-of-the-art [$^{64/67}$Cu]Cu^{2+} chelators are given in Table S5 (ESI†).

Surprisingly, TACD3S gave a very low pCu^{2+} demonstrating it was not able to complex Cu^{2+} except at nearly neutral pH. It follows that the copresence of four nitrogen atoms is an essential feature in a 12-member macrocyclic structure to allow an effective copper coordination when the side chains contain S donors, as the removal of a nitrogen donor and a sulfur side chain have a huge impact on the Cu^{2+} coordination. This low Cu^{2+}–complex stability hampered any further investigation with TACD3S, so that this ligand will no longer be considered in the following discussion.

The addition of a ring carbon atom in the DO4S scaffold, leading to TRI4S, only slightly affects the complex stability at physiological pH (pCu^{2+} 17.0 for TRI4S and 17.7 for DO4S, Table 2).[27] Contrarily, the further increase of the ring size, leading to TE4S, is detrimental in terms of the stability of the resulting Cu^{2+} complexes, as the pCu^{2+} of TE4S is 2.5 orders of magnitude lower than that of TRI4S. These behaviours are likely related to the worst matching between the size of the metal cation and ring cavity, thus resulting in a stability drop.

Table 2 Overall stability constants ($\log\beta$) and pCu values of the Cu^{2+} and Cu^{+} complexes formed by TACD3S, TRI4S and TE4S at I = 0.15 M NaCl and T = 25 °C. Literature data for $Cu^{2+/+}$–DO4S are reported for comparison purposes. Unless otherwise stated, $\log\beta$ for Cu^{2+} were obtained by UV-Vis spectrophotometric titrations whereas those for Cu^{+} were computed from cyclic voltammetry[a]

Ligand	TACD3S	DO4S[d]	TRI4S	TE4S
$\log\beta$ Cu^{2+}	6.6 ± 0.4	19.8	18.53 ± 0.04	17.24 ± 0.07; 17.01 ± 0.02[c]
pCu^{2+} [b]	6.2	17.7	17.0	14.5
$\log\beta$ Cu^{+}	—	19.8	16.8 ± 0.1	16.3 ± 0.1
pCu^{+} [b]	—	17.2	15.3	13.6

[a] L denotes the ligand in its totally deprotonated form. The reported uncertainty was obtained by the fitting procedure and represents one standard deviation unit. [b] $pCu^{2+/+}$ calculated at $C_{Cu^{2+/+}} = 10^{-6}$ M and $C_L = 10^{-5}$ M at pH = 7.4 using the constants of Tables 1 and 2 or taken from ref. 27. [c] Obtained by pH-potentiometric titrations, I = 0.15 M $NaNO_3$. [d] From ref. 27.

Cu^{2+} complexes: electronic and EPR structural analysis

The analysis of the electronic spectra of the investigated Cu^{2+} complexes allowed us to evaluate the structural changes induced by the ring size increase. A comparison between the UV-Vis spectra of the Cu^{2+}–DO4S, Cu^{2+}–TRI4S and Cu^{2+}–TE4S complexes is reported in Fig. 3. The involvement of the chloride anions in the Cu^{2+} coordination sphere is negligible for both Cu^{2+}–TRI4S and Cu^{2+}–TE4S as the spectra measured upon the addition of an excess of NaCl (I = 0.15 M) to aqueous solutions (I = 0 M) do not change (Fig. S19, ESI†).

Cu^{2+}–TRI4S displays a strongly intense UV transition at 313 nm accompanied by a less intense single broad band in the visible region at 598 nm (Table S6, ESI†). This band set is very similar to the one previously obtained for Cu^{2+}–DO4S,[27] so that the same structural features can be hypothesized in both cases.

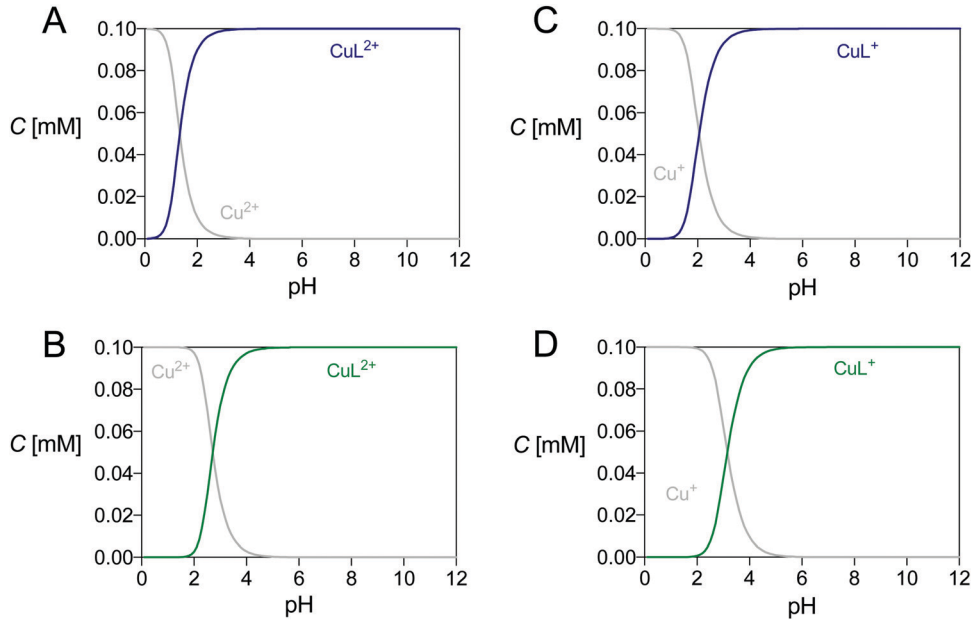

Fig. 2 Distribution diagrams of (A) Cu^{2+}–TRI4S, (B) Cu^{2+}–TE4S, (C) Cu^{+}–TRI4S and (D) Cu^{+}–TE4S. The plots were calculated from the overall stability constants reported in Tables 1 and 2 at $C_{Cu} = C_L = 1.0 \times 10^{-4}$ M.

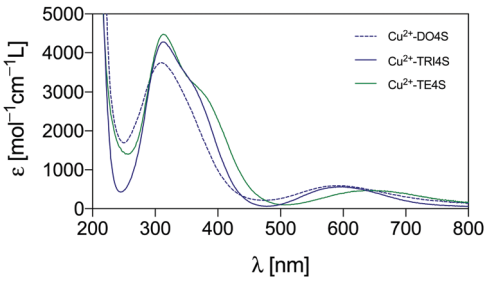

Fig. 3 Comparison of the normalized electronic spectra of the cupric complexes with DO4S, TRI4S and TE4S (ε = absorbivity coefficient). The electronic spectrum of the Cu–DO4S system was taken from ref. 27.

In particular, two different isomers having either $[4N]S_{ax}$ or [4N] coordination arrangements might exist in solution with TRI4S, as was found for the cupric complex of DO4S.[27] When turning to Cu^{2+}–TE4S, the maximum absorption is maintained (Table S6, ESI†), but a remarkable increase of the shoulder at 370 nm accompanied with a redshift of the *d–d* band (from 598 nm to 626 nm) can be observed, thus suggesting that TE4S binds Cu^{2+} through a different coordination mode.

To further investigate this result, EPR analysis was carried out for Cu^{2+}–TE4S solutions. The EPR spectra recorded at room temperature showed the appearance of free copper ion only below pH 2 (Fig. 4). At higher pH, the CuL^{2+} complex spectra were measured, and no further spectral changes were detected, in agreement with the speciation model (Table 2, Fig. 2). In frozen solution, the complex becomes predominant at higher pH, and at pH 2.76, ~ 30% free copper was detected. The component ratios are shown in Fig. S20 (ESI†).

The obtained EPR parameters are reported in Table 3. The parameters for Cu^{2+}–TE4S are close to those of Cu^{2+}–DO4S isomer (2), reported in our previous work, where the coordination of the macrocycle is driven by four nitrogen and complemented axially by a sulfide side chain (Table 3). However, for Cu^{2+}–TE4S a significantly higher $A_\perp$ was detected.[27] This is probably due to the higher symmetrical arrangement of the nitrogen donor atoms in the equatorial sphere, which makes the copper centre in plane with the nitrogen atoms, resulting in higher copper hyperfine coupling values. The observed redshift in the UV-Vis spectra of Cu^{2+}–TE4S, when compared to Cu^{2+}–DO4S, could be therefore rationalized considering that the UV-Vis spectrum of the latter is a mixture of the spectra deriving from two components, [4N] and $[4N]S_{ax}$,[27] while Cu^{2+}–TE4S contains only $[4N]S_{ax}$. This result is in perfect agreement with the data obtained by Schmidt *et al.* in the solid-state, as their Cu^{2+}–TE4S crystal, when investigated by X-ray, was also demonstrated to possess a $[4N]S_{ax}$ structure.[29]

The significantly distended Cu^{2+} cation in the cyclam backbone indicates a mismatch within the ligand metal-binding cleft which could be correlated to the lower thermodynamic stability when compared to DO4S (Table 2).

Cu^{2+} complexes: dissociation kinetics

Promising BFC candidates for radiopharmaceutical applications must exhibit high thermodynamic stability at physiological pH, but also high kinetic inertness toward dissociation.[21]

The kinetic inertness of the Cu^{2+}–TRI4S and Cu^{2+}–TE4S complexes were at first evaluated in the presence of an excess of competitor cations, *i.e.* Ni^{2+} and Zn^{2+}, by studying the species evolution with time after the competitor additions. Ni^{2+} and Zn^{2+} were chosen as they are common metallic impurities in radiocopper solutions, and Zn^{2+} also represents a biologically relevant cation.[21] In all cases, only minor decomplexation was observed within 5 days, as indicated by the slight decrease of

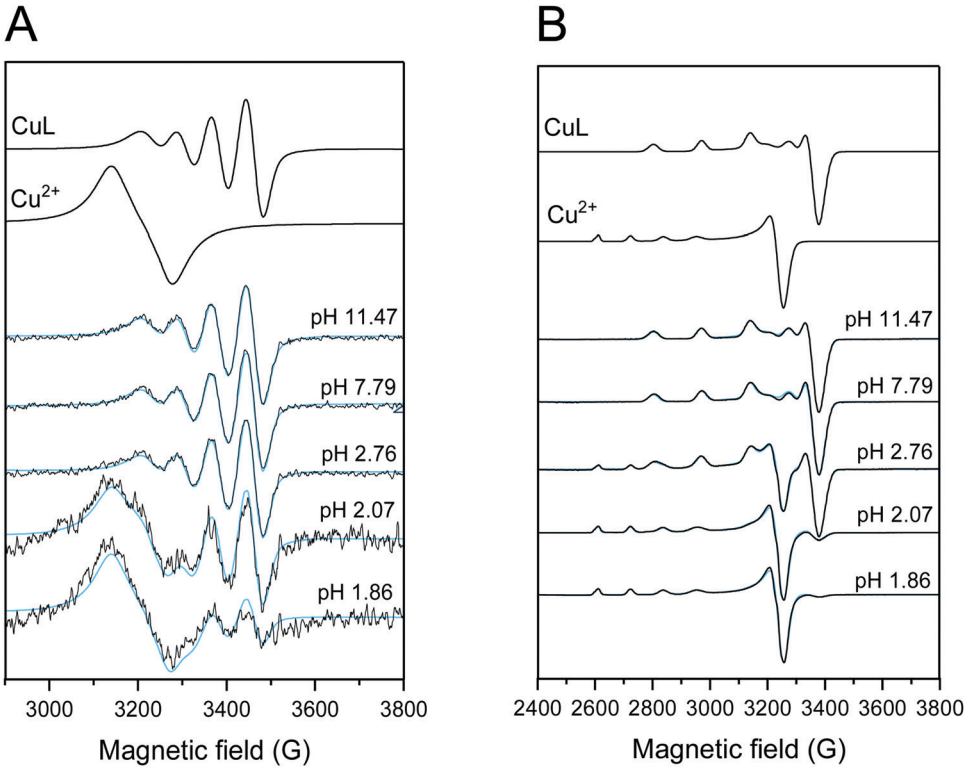

Fig. 4 Experimental (black) and simulated (light blue) EPR spectra of solutions containing Cu^{2+} and TE4S ($C_{Cu^{2+}} = 8.7 \times 10^{-4}$ M, $C_{TE4S} = 1.08 \times 10^{-3}$ M) at (A) room temperature and (B) 77 K. The component spectra obtained from the simulation are shown in the upper part (the spectral intensities were normalized).

Table 3 Calculated isotropic and anisotropic EPR parameters obtained by the simulation of room temperature and frozen solution spectra of Cu^{2+}–TE4S

	Isotropic parameters[a]		Anisotropic parameters[b]				Calculated[c]
	g_0	A_0 [$\times 10^4 cm^{-1}$]	$g_\perp$	$g_\parallel$	$A_\perp$ [$\times 10^{-4} cm^{-1}$]	$A_\parallel$ [$\times 10^{-4} cm^{-1}$]	$g_{0,calc}$
$Cu_{(aq)}$	2.194	34.1	2.084	2.423	4.9	126.1	2.197
Cu^{2+}–TE4S	2.101	73.3	2.048	2.204	38.2	168.1	2.100
Cu^{2+}–DO4S (2)[d]	2.103	63.6	2.048, 2.058	2.209	20.3, 23.5	171.2	2.105

[a] The experimental error was ± 0.001 for g_0 and ± 1 × 10^{-4} cm^{-1} for A_0. [b] The experimental error was ± 0.002 for $g_\perp$ and ± 0.001 for $g_\parallel$ and ± 1·10^{-4} cm^{-1} for $A_\perp$ and $A_\parallel$. [c] Calculated by the equation $g_{0,calc} = (2g_\perp + g_\parallel)/3$ on the basis of anisotropic values. [d] From ref. 27.

the absorption in the electronic spectra of the two cupric complexes (Fig. S21 and S22, ESI†): the percentages of intact complexes are reported in Tables S7 and S8 (ESI†) and they were always > 90%. These results can be related to an interplay between a marked kinetic inertness of the investigated Cu^{2+} complexes in the tested conditions and a not very high thermodynamic stability of the corresponding Zn^{2+} and Ni^{2+} complexes. The latter was qualitatively evaluated by ^{1}H-NMR or UV-Vis spectra as briefly described in the captions of Fig. S23 and S24 (ESI†).

The inertness of the Cu^{2+}–TRI4S and Cu^{2+}–TE4S complexes was also investigated in harsher conditions than above, by evaluating the acid-assisted dissociation kinetics. Albeit this assay could not predict the *in vivo* integrity of the resulting complex, it is considered a convenient and popular gauge of relative kinetic inertness of copper–tetraamine complexes to Cu^{2+} decomplexation in aqueous media and as a first screening for monitoring the Cu^{2+}–chelator stability.[46–48] Also, the first generation ligands DO4S and DO2A2S were tested through these assays for comparison purposes.

Representative data are shown in Fig. S25–S28 (ESI†). The experimentally observed dissociation rate constants ($^dk_{obs}$) and the corresponding half-life ($t_{1/2}$) at different HCl concentrations are compiled in Tables S9 and S10 (ESI†), respectively. For DO4S and DO2A2S, the $^dk_{obs}$ values linearly change with the proton content (Fig. S29, ESI†), indicating that only one complex undergoes dissociation, and that the protonation constant of the predissociation step is low.[49,50] The second-order rate constant (^dk) was thus obtained using $^dk_{obs} = {}^dk[H^+]$ as the fitting equation. In the case of TRI4S, the $^dk_{obs}$ *vs.* $[H^+]$ dependence was not

apparently linear, and a negative intercept was obtained, so that the above-stated conditions do not apply. If two paths are assumed to coexist, involving the addition of one and of two protons, respectively, the equation $^{d}k_{obs} = {}^{d}k[H^+] + {}^{d}k_2[H^+]^2$ represents a better model.[50] Therefore, we have used this equation (Fig. S29, ESI†), from which the constants given in Table S10 (ESI†) were obtained.

The dissociation kinetics of the Cu^{2+} complexes strongly depends on the ligand side arms: Cu^{2+}–DO2A2S is the most inert, likely due to the presence of coordinated carboxylates in the ligand structure, either in protonated or unprotonated form. Likely, the sulfur arms do not provide a significant contribution to the kinetic inertness of the Cu^{2+} complexes: this can be deduced if the ^{d}k value of Cu^{2+}–DO4S is compared with those of Cu^{2+}–cyclen and Cu^{2+}–DOTA given in the literature ($^{d}k = \sim 5 \times 10^{-4}$ and 6×10^{-6} s^{-1}, respectively).[51] Moreover, the obtained results demonstrated that the ring dimension makes the difference in the inertness of the Cu^{2+} complexes, because the Cu^{2+} complex formed by DO4S is kinetically much more inert than those formed by TRI4S and TE4S. The contrast between related cyclen- and cyclam-based complexes is dramatic since the Cu^{2+}–TE4S complex dissociates within minutes (Table S10, ESI†) even at the lowest HCl concentrations (due to the few experimental points and the high speed of the dissociation, only a rough ^{d}k value of $\sim 10^{-2}$ M^{-1} s^{-1} can be given for this ligand). Thus, the increase in the ring size not only affects the thermodynamic stability but also the acid-assisted dissociation behaviour of these complexes. If the results of Table 2 and Table S10 (ESI†) are compared, it follows that the decomplexation rates of the cupric complex in highly acidic solution are strongly correlated with the complex stabilities. For example, this correlation is clearly visible in Fig. S30 (ESI†) where pCu^{2+} values at physiologic pH are plotted *vs.* $\log(t_{1/2})$ at pH 1.

Cu^+ complexes: cyclic voltammetry, solution thermodynamics and structural analysis

A cyclic voltammetry (CV) study was undertaken in water using 0.15 M $NaNO_3$ as a supporting electrolyte to evaluate the stabilities of the investigated complexes upon reduction to Cu^+.

The electrochemical behaviour of the unbound TRI4S and TE4S was firstly assessed. Both ligands were demonstrated to be electrochemically inactive in the potential range of the Cu^{2+}/Cu^+ pair, *i.e.* from +0.5 to −0.5 V *vs.* SCE (Fig. S31, ESI†). The CV of the unbound Cu^{2+} was acquired using the same experimental conditions: two poorly separated cathodic peaks, followed by an anodic stripping peak in the backward scan were observed (Fig. S32, ESI†). Stepwise reduction of Cu^{2+} to electrodeposited Cu^0 occurs in the forward scan, while the latter is anodically stripped from the electrode upon scan reversal.

Representative cyclic voltammograms of the Cu complexes with TRI4S and TE4S acquired at physiological pH and different scan rates are shown in Fig. 5, while the electrochemical properties of their Cu complexes are listed in Table 4.

The copper complexes of both ligands displayed a redox process ascribed to a quasi-reversible one-electron reduction of Cu^{2+} to Cu^+ (Fig. 5) at $E_{1/2,\ Cu\text{-}TRI4S} = -0.223 \pm 0.003$ V *vs.* SCE and $E_{1/2,\ Cu\text{-}TE4S} = -0.170 \pm 0.003$ *vs.* SCE. The peak separation (ΔE_p) was higher than the canonical 60 mV for Nernstian electron transfer (ET) processes (Table 4), indicating that the ET are quasi-reversible. The voltammetric pattern was unchanged with multiple reduction/oxidation cycles and at the different scan rates (Fig. 5): in both cases, a linearity between the intensity of the cathodic peak current (i_{pc}) and the square root of the scan rate ($\nu^{1/2}$) was found (Fig. S33, ESI†), indicating that the electrode process is under diffusion control.

The complex formed between Cu^+ and both ligands at pH 7 was assumed to be CuL^+ because the "first-generation" ligands form this complex under the same conditions.[27] This was further confirmed from cyclic voltammograms acquired at different pH which do not show any pH-dependent variation of their pattern (Fig. S34, ESI†). The stability constants of each CuL^+ complex were determined as described in our previous work.[27] Briefly, a thermodynamic cycle was used, which involved the stability constant of the Cu^{2+} complex ($Cu^{2+}L$), and the standard potential (E^0) for the $Cu^{2+} + e^- \rightarrow Cu^+$ and $Cu^{2+}L + e^- \rightarrow Cu^+L$ semi-reactions (assuming that the experimental $E_{1/2}$ values approximate the E^0). The corresponding free Gibbs energies were summed to obtain the unknown stability constant of Cu^+L. The results are detailed in Table 2 and the corresponding distribution diagrams are shown in Fig. 2.

The calculated pCu^+ values ($pCu^+ = -\log[Cu^+]_{free}$) reported in Table 2 indicate that the increase of the ring size from a

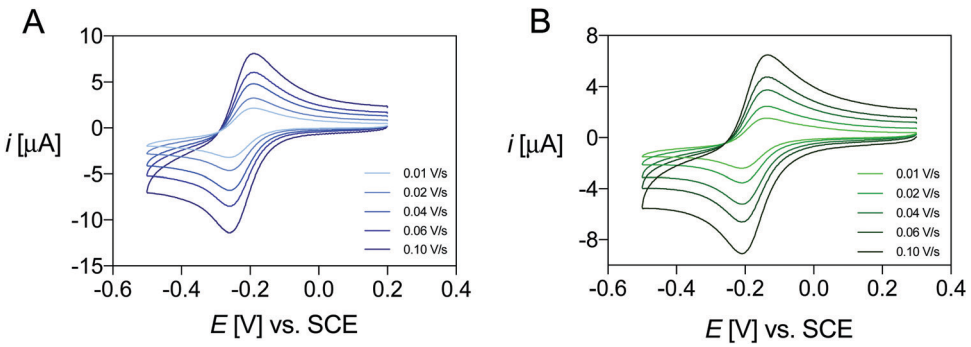

Fig. 5 Representative cyclic voltammograms of the copper complexes of (A) TRI4S ($C_{Cu^{2+}} = 8.0 \times 10^{-4}$ M, $C_{TRI4S} = 1.0 \times 10^{-3}$ M) and (B) TE4S ($C_{Cu^{2+}} = 8.0 \times 10^{-4}$ M, $C_{TE4S} = 1.1 \times 10^{-3}$ M) in aqueous solution at physiological pH, I = 0.15 M $NaNO_3$ and T = 25 °C acquired at different scan rates.

Table 4 Electrochemical data (E_{pc} = cathodic peak potential, E_{pa} = anodic peak potential, ΔE_p = peak separation, $E_{1/2}$ = half-wave potential) obtained for the copper complexes of TRI4S and TE4S in aqueous solutions at I = 0.15 M $NaNO_3$ and T = 25 °C

System[a]	E_{pc} [V] *vs.* SCE	E_{pa} [V] *vs.* SCE	ΔE_p [mV] *vs.* SCE	$E_{1/2}$ [V] *vs.* SCE
Cu–TRI4S	−0.269 ± 0.001	−0.177 ± 0.006	91	−0.223 ± 0.003
Cu–TE4S	−0.216 ± 0.003	−0.125 ± 0.004	91	−0.170 ± 0.003

[a] Average of the values measured at 0.01 V $s^{-1} \leq \nu \leq$ 0.1 V s^{-1}.

12-(DO4S) to a 13-(TRI4S) and then to a 14-member macrocycle (TE4S) corresponds to a progressive decrease of the Cu^+ complexes stability, likewise to what was found for the +2 oxidation state (Table 2). It can also be observed that the pCu^+ for DO4S is considerably higher than the pAg^+ determined in our previous work[28] (17.2 *vs.* 14.5), and preliminary data about silver complexation (in due course in our laboratories) indicate that a similar trend exists also for TRI4S and TE4S. It is known that polyamines coordinate Cu^+ more strongly than Ag^+: for example, Cu^+ forms complexes in aqueous solution with both ethylenediamine and triethylenetetramine which are three orders of magnitude more stable than those formed by Ag^+.[52] This stability difference appears to be retained by our ligands, thus indicating that the thioethers in the coordination sphere do not show specific preference for either Cu^+ or Ag^+.

The reversibility of the CV process suggests that all electrogenerated cuprous complexes are stable and do not dissociate during the CV timescale. The long-term stability of the CuL^+ complexes was then further confirmed by controlled-potential electrolysis of the Cu^{2+} complexes. Linear-scan voltammetry (LSV) was employed to monitor the reduction processes (Fig. S35, ESI†). It was evidenced that the CuL^+ complexes formed by both ligands remained stable at least for some hours after their *in situ* formation by CuL^{2+} reduction. These results demonstrate the ability of TRI4S and TE4S to adapt to both the Cu^{2+} and Cu^+ coordination requirements, analogously to what we have previously found with DO4S.[27] A donor switching can be expected upon copper reduction, as reported for a number of similar polyazamacrocycles.[53]

The CV data also allow us to obtain information on the ability of the investigated complexes to resist the demetallation process that could be induced *in vivo* by the biologically triggered redox switching between Cu^{2+} and Cu^+. The standard reduction potentials of the Cu^{2+} complexes were calculated as $E_{1/2} = (E_{pc} + E_{pa})/2$ and assuming that $E_{1/2} = E^0$. The reduction potentials for Cu^{2+}–TRI4S and Cu^{2+}–TE4S (Table 4) are higher than the estimated potential threshold for typical bioreductants (E^0 = −0.64 V *vs.* SCE), which indicates that they would be vulnerable to *in vivo* reduction.[27,54] Indeed, the short- and the long-term stability observed in the voltammetric and electrolytic measurements suggests that the resulting Cu^+ complex would not undergo demetallation and so the copper would remain anchored to the radiopharmaceutical.

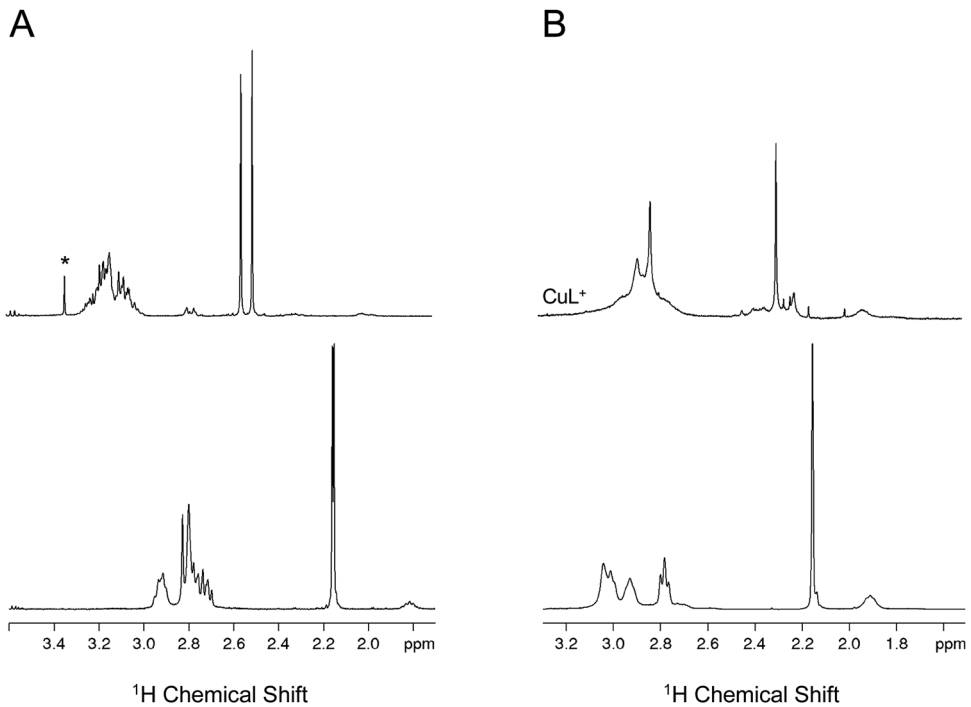

Fig. 6 ^{1}H NMR spectra (400 MHz, 25 °C, H_2O + 10% D_2O) of the *in situ* generated Cu^+ complexes of (A) TRI4S (C_{Cu} = 8.0 × 10^{-4} M, C_{TRI4S} = 1.0 × 10^{-3} M, pH 7) and (B) TE4S (C_{Cu} = 6.0 × 10^{-4} M, C_{TRI4S} = 7.0 × 10^{-3} M, pH 8), and comparison with the ^{1}H NMR spectra of the unbound ligands with the same net charge. The signal marked with an asterisk is related to a methanol impurity.

Thanks to their long-term stability, the Cu^{+}–TRI4S and Cu^{+}–TE4S solutions obtained after electrolysis at pH ~ 7 and ~ 8, respectively, were characterized by ^{1}H-NMR measurements. ^{1}H NMR spectra of the Cu^{+} complexes, compared with the spectra of the free ligands, are reported in Fig. 6. The signals assignment is presented in Table S11 (ESI†), supported by the TOCSY spectra in the case of Cu^{+}–TE4S (Fig. S36, ESI†).

The significant changes in chemical shift and coupling pattern observed among the spectra of the free ligands and those of the Cu^{+} complexes undoubtedly confirm the complexation event. All the signals experience a downfield shift upon complexation (more pronounced in the case of Cu^{+}–TRI4S) likely because of the electron density donation from the ligand to the metal ion, thereby suggesting that all the donors are interacting on average with Cu^{+}.

For Cu^{+}–TRI4S, the SCH_3 protons of the side chains resonate as two narrow singlets with the same intensity at 2.50 and 2.55 ppm (Table S11, ESI†). This, combined with the observed downfield shift, is consistent with the involvement of the S donors in the coordination of Cu^{+}. Their two-by-two equivalence likely reflects the intrinsic asymmetry of the ligand.

For Cu^{+}–TE4S, the methyl groups of the side chains (SCH_3) resonate as a singlet at 2.29 ppm, thus indicating that also in this case the S atoms are involved in the coordination sphere of the metal ion. For both ligands, the S donors can be simultaneously bound to the metal ions, or in rapid exchange with respect to the NMR timescale.

The signals of the SCH_2 and NCH_2 protons of the side chains and the ring resonate as non-resolved multiplets in both cases (Table S11, ESI†). The main difference between the NMR spectra of Cu^{+}–TRI4S and Cu^{+}–TE4S is that the latter has broader signals, suggesting that the Cu^{+}–TE4S complex is more fluxional and/or its conformational equilibria are slower.

The multiplet attributed to the methylene protons of the propylenic chain of the ring is split into two broad signals of equal relative integral only when Cu^{+} is coordinated by TRI4S; these two signals have been attributed to the axial and equatorial protons of the same molecule, which for conformational constraint become non-magnetically equivalent.

Conclusions

The stabilization of coordinatively labile and redox-active copper ions in biological environments remains a challenge for the development of improved diagnostic and therapeutic strategies with [$^{64/67}$Cu]Cu^{2+}, as the *in vivo* integrity of these complexes could be thwarted by the bio-induced reduction of Cu^{2+} to Cu^{+} that may result in demetallation processes. The *N*-functionalized cyclen derivatives listed in Fig. 1, bearing borderline N and soft S donors, were considered in our previous work in an attempt to stabilize both oxidation states.[27]

Subtle changes in the ligand structure and donor arms can cause drastic changes to the stability of their radiometal complexes, so that the effects induced by the modification of the azamacrocyclic ring on the physicochemical properties of the corresponding Cu^{2+} and Cu^{+} complexes were investigated herein. As a consequence of the larger ring size with respect to the previously developed 12-member sulfanyl analogue (DO4S), TRI4S and TE4S present a faster complexation process than DO4S, which is a feature of particular interest for radiopharmaceutical applications. The stability of the Cu^{2+} complexes demonstrated that the increase of one carbon in the azamacrocyclic ring has a negligible influence, as TRI4S and DO4S form complexes of comparable stability. However, a further increase in the ring size leading to TE4S results in a noticeable drop in the stability constants and the corresponding pCu^{2+} values. The same trend was observed as regards their inertness towards acid-mediated decomplexations and the stability of their Cu^{+} complexes. The number of nitrogen donors has a major influence on the stability of the Cu^{2+} complexes, at least for ring sizes larger than or equal to 12, as TACD3S was not able to strongly stabilize the metal cation.

On the other hand, the changing ring size did not affect the exceptional inertness of the copper complexes in reductive media as revealed by cyclic voltammetry and electrolysis experiments. While the $E_{1/2}$ still make these Cu^{2+}-complexes susceptible to *in vivo* reduction, no subsequent Cu^{+} loss should occur.

Radiolabelling, *in vitro* and *in vivo* experiments, although out of the scope of the present paper, will be necessary in order to validate the potential of these ligands for future radiopharmaceutical applications.

Author contributions

Marianna Tosato: conceptualization, formal analysis, investigation, methodology, writing – original draft, writing – review & editing. Matteo Pelosato: investigation (potentiometry, UV-Vis, NMR, cyclic voltammetry). Sara Franchi: investigation (potentiometry, UV-Vis). Abdirisak Ahmed Isse: investigation (cyclic voltammetry). Nóra Veronica May: investigation (EPR), funding acquisition. Giordano Zanoni: investigation (synthesis). Fabrizio Mancin: investigation (synthesis). Paolo Pastore: formal analysis (cyclic voltammetry), funding acquisition, resources. Denis Badocco: formal analysis (cyclic voltammetry). Mattia Asti: supervision, formal analysis. Valerio Di Marco: supervision, data curation, formal analysis, methodology, project administration, writing – review & editing.

Conflicts of interest

There are no conflicts to declare.

Acknowledgements

This research work was supported by the ISOLPHARM_EIRA project funded by the Legnaro National Laboratories of the Italian Institute of Nuclear Physics (*Istituto Nazionale di Fisica Nucleare – Laboratori Nazionali di Legnaro*, INFN-LNL, Italy) and by the National Research, Development and Innovation Office-NKFIA (Hungary) through project K124544.

References

1 A. Yordanova, E. Eppard, S. Kürpig, R. A. Bundschuh, S. Schönberger, M. Gonzalez-Carmona, G. Feldmann, H. Ahmadzadehfar and M. Essler, *OncoTargets Ther.*, 2019, **10**, 4821–4828.

2 E. Boros, J. F. Cawthray, C. L. Ferreira, B. O. Patrick, M. J. Adam and C. Orvig, *Inorg. Chem.*, 2012, **51**, 6279–6284.

3 N. M. Di Bartolo, A. M. Sargeson, T. M. Donlevya and S. V. Smith, *J. Chem. Soc., Dalton Trans.*, 2001, 2303–2309.

4 M. Shokeen and C. J. Anderson, *Acc. Chem. Res.*, 2009, **42**, 832–841.

5 E. Boros and A. B. Packard, *Chem. Rev.*, 2019, **119**, 870–901.

6 F. Borgna, M. Ballan, C. Favaretto, M. Verona, M. Tosato, M. Caeran, S. Corradetti, A. Andrighetto, V. Di Marco, G. Marzaro and N. Realdon, *Molecules*, 2018, **23**, 2437.

7 G. Hao, T. Mastren, W. Silvers, G. Hassan, O. K. Öz and X. Sun, *Sci. Rep.*, 2021, **11**, 3622.

8 I. Carbo-Bague and C. F. Ramogida, in *Encyclopedia of Inorganic and Bioinorganic Chemistry*, R. A. Scott., 2021.

9 C. Ramogida and C. Orvig, *Chem. Commun.*, 2013, **49**, 4720–4739.

10 T. I. Kostelnik and C. Orvig, *Chem. Rev.*, 2019, **119**, 902–956.

11 E. W. Price and C. Orvig, *Inorg. Chem.*, 2014, **43**, 260–290.

12 K. S. Woodin, K. J. Heroux, C. A. Boswell, E. H. Wong, G. R. Weisman, W. Niu, S. A. Tomellini, C. J. Anderson, L. N. Zakharov and A. L. Rheingold, *Eur. J. Inorg. Chem.*, 2005, 4829–4933.

13 A. Guillou, L. M. P. Lima, M. Roger, D. Esteban-Gomez, R. Delgado, C. Platas-Iglesias, V. Patinec and R. Tripier, *Eur. J. Inorg. Chem.*, 2017, 2435–2443.

14 S. Bhattacharyya and M. Dixit, *Dalton Trans.*, 2011, **40**, 6112–6128.

15 N. Camus, N. Le Bris, S. Nuryyeva, M. Chessé, D. Esteban-Gómez, C. Platas-Iglesias, R. Tripier and M. Elhabiri, *Dalton Trans.*, 2017, **46**, 11479–11490.

16 M. Le Fur, M. Beyler, N. Le Poul, L. M. P. Lima, Y. Le Mest, R. Delgado, C. P. Iglesias, V. Patinec and R. Tripier, *Dalton Trans.*, 2016, **45**, 7406–7420.

17 E. Bodio, M. Boujtita, K. Julienne, P. Le Saec, S. G. Gouin, J. Hamon, E. Renault and D. Deniaud, *ChemPlusChem*, 2014, **79**, 1284–1293.

18 S. Shuvaev, E. A. Suturina, N. J. Rotile, C. A. Astashkin, C. J. Ziegler, A. W. Ross, T. L. Walker, P. Caravan and I. S. Taschner, *Dalton Trans.*, 2020, **49**, 14088–14098.

19 M. S. Cooper, M. T. Ma, K. Sunassee, K. P. Shaw, J. D. Williams, R. L. Paul, P. S. Donnelly and P. J. Blower, *Bioconjugate Chem.*, 2012, **23**, 1029–1039.

20 L. M. Lima, D. Esteban-Gomez, R. Delgado, C. Platas-Iglesias and R. Tripier, *Inorg. Chem.*, 2012, **51**, 6916–6927.

21 R. Gillet, A. Roux, J. Brandel, S. Huclier-Markai, F. Camerel, O. Jeannin, A. M. Nonat and L. J. Charbonniere, *Inorg. Chem.*, 2017, **56**, 11738–11752.

22 E. Boros, E. Rybak-Akimova, J. P. Holland, T. Rietz, N. Rotile, F. Blasi, H. Day, R. Latifi and P. Caravan, *Mol. Pharmaceutics*, 2014, **11**, 617–629.

23 T. J. Wadas, E. H. Wong, G. R. Weisman and C. J. Anderson, *Curr. Pharm. Des.*, 2007, **13**, 3–16.

24 D. J. Stigers, R. Ferdani, G. R. Weisman, E. H. Wong, C. J. Anderson, J. A. Golen, C. Moore and A. L. Rheingold, *Dalton Trans.*, 2010, **39**, 1699–1701.

25 C. Gotzmann, F. Braun and M. D. Bartholomä, *RSC Adv.*, 2016, **6**, 119–131.

26 R. Ševčík, J. Vaněk, R. Michalicová, P. Lubal, P. Hermann, I. C. Santos, I. Santos and M. P. C. Campello, *Dalton Trans.*, 2016, **45**, 12723–12733.

27 M. Tosato, M. Dalla Tiezza, N. V. May, A. A. Isse, S. Nardella, L. Orian, M. Verona, C. Vaccarin, A. Alker, H. Mäcke, P. Pastore and V. Di Marco, *Inorgan. Chem.*, 2021, **60**, 11530–11547.

28 M. Tosato, M. Verona, R. Doro, M. Dalla Tiezza, L. Orian, A. Andrighetto, P. Pastore, G. Marzaro and V. Di Marco, *New J. Chem.*, 2020, **44**, 8337–8350.

29 C. L. Schmid, M. Neuburger, M. Zehnder, T. A. Kaden, K. Bujno and R. Bilewicz, *Helv. Chim. Acta*, 1997, **80**, 241–252.

30 S. Lacerda, M. P. Campello, I. C. Santos, I. Santos and R. Delgado, *Polyhedron*, 2007, **26**, 3763–3773.

31 R. Ševčíková, P. Lubal, M. P. C. Campello and I. Santos, *Polyhedron*, 2013, **62**, 268–273.

32 S. Lacerda, M. P. Campello, F. Marques, L. Gano, V. Kubiček, P. Fousková, É. Tóth and I. Santos, *Dalton Trans.*, 2009, 4509–4518.

33 R. Ma, M. J. Welch, J. Reibenspies and A. E. Martell, *Inorg. Chim. Acta*, 1995, **236**, 75–82.

34 M. Tosato, M. Asti, M. Dalla Tiezza, L. Orian, D. Häussinger, R. Vogel, U. Köster, M. Jensen, A. Andrighetto, P. Pastore and V. Di Marco, *Inorg. Chem.*, 2020, **59**, 10907–10919.

35 T. L. Hwang and A. J. Shaka, *J. Magn. Reson., Ser. A*, 1995, **112**, 275–279.

36 V. Di Marco, PhD thesis, University of Padova, 1998.

37 L. G. Sillen, *Acta Chem. Scand.*, 1964, **18**, 1085.

38 W. H. Press, B. P. Flannery, S. A. Teukolsky and W. T. Vetterling, *Numerical Recipes: The Art of Scientific Computing*, Cambridge University Press, 1986.

39 C. F. Baes Jr. and R. E. Mesmer, *The Hydrolysis of cations*, New York, 1976.

40 A. Rockenbauer and L. Korecz, *Appl. Magn. Reson.*, 1996, **10**, 29–43.

41 L. J. Zompa, *Inorg. Chem.*, 1978, **17**, 2531–2536.

42 M. Kodama and E. Kimura, *J. Chem. Soc., Dalton Trans.*, 1976, 1720–1724.

43 A. Bianchi, M. Micheloni and P. Paoletti, *Coord. Chem. Rev.*, 1991, **110**, 17–113.

44 B. S. Nakani, J. J. B. Welsh and R. D. Hancock, *Inorg. Chem.*, 1983, **22**, 2956–2958.

45 M. Tosato and V. Di Marco, *Biomolecules*, 2019, **9**, 269.

46 J. Kotek, P. Lubal, P. Hermann, I. Císarová, I. Lukes, T. Godula, I. Svobodová, P. Táborský and J. Havel, *Chem. – Eur. J.*, 2003, **9**, 233–248.

47 H. Aneetha, Y. H. Lai, S. C. Lin, K. Panneerselvam, T. H. Lu and C. S. Chung, *J. Chem. Soc., Dalton Trans.*, 1999, 2885–2892.

48 A. V. Dale, G. I. An, D. N. Pandya, Y. S. Ha, N. Bhatt, N. Soni, H. Lee, H. Ahn, S. Sarkar, W. Lee, P. T. Huynh, J. Y. Kim, M. R. Gwon, S. H. Kim, J. G. Park, Y. R. Yoon and J. Yoo, *Inorg. Chem.*, 2015, **54**, 8177–8186.
49 V. Kubíček, Z. Böhmová, R. Ševčíková, J. Vaněk, P. Lubal, Z. Poláková, R. Michalicová, J. Kotek and P. Hermann, *Inorg. Chem.*, 2018, **57**, 3061–3072.
50 M. Paúrová, T. David, I. Císařová, P. Lubal, P. Hermann and J. Kotek, *New J. Chem.*, 2018, **42**, 11908–11929.
51 I. Voráčová, J. Vaněk, J. Pasulka, Z. Střelcová, P. Lubal and P. Hermann, *Polyhedron*, 2013, **61**, 99–104.
52 P. D. Bernardo, A. Melchior, R. Portanova, M. Tolazzi and P. L. Zanonato, *Coord. Chem. Rev.*, 2008, **252**, 1270–1285.
53 D. B. Rorabacher, *Chem. Rev.*, 2004, **104**, 651–698.
54 A. Rodríguez-Rodríguez, Z. Halime, L. M. P. Lima, M. Beyler, D. Deniaud, N. Le Poul, R. Delgado, C. Platas-Iglesias, V. Patinec and R. Tripier, *Inorg. Chem.*, 2016, **55**, 619–632.